


New extraction of the nucleon charge radius based on its Dirac-flavor-dependent form factors

M. A. Albloushi , I. A. Qattan *, and S. Shoeibi

Department of Physics, *Khalifa University of Science and Technology*, P.O. Box 127788, Abu Dhabi, United Arab Emirates



(Received 9 December 2023; revised 26 February 2024; accepted 1 May 2024; published 5 June 2024)

In this work, we present new extractions of the proton $\langle r_p \rangle$ and neutron $\langle r_n^2 \rangle$ root-mean-square charge radius using the Dirac flavor-separated up- and down-quark $F_1^{(u,d)}(Q^2)$ form factors data covering the range $0.0155 < Q^2 < 4.250 \text{ GeV}^2$ from I. A. Qattan and J. Arrington [Phys. Rev. C **86**, 065210 (2012)] and I. A. Qattan, J. Arrington, and A. Alsaad [Phys. Rev. C **91**, 065203 (2015)]. The charge radius values are calculated using the two-dimensional (2D) transverse quark charge distributions based on the slopes of $F_1^{(u,d)}(Q^2)$ at $Q^2 = 0$ through model-independent relations. As the charge radius is extracted in the limit $Q^2 \rightarrow 0$ with focus mainly on low- Q^2 data points, we limit our extraction up to $Q^2 = 1.0 \text{ GeV}^2$, and investigate the impact of fitting procedure, data fitting range, and convergence of the fitted functions used on the stability and precision of the extracted charge radius. In addition, we investigate any model dependence of the fits that might be associated with the inclusion of high- Q^2 data points by extending the fitting range up to $Q^2 = 4.25 \text{ GeV}^2$. For the proton, we find $\langle r_p \rangle = 0.848 \pm 0.002(\text{stat.}) \pm 0.003(\text{sys.}) \text{ fm}$, which is in excellent agreement with the ultra-high precise muonic hydrogen μH Lamb shift results and PRad I Collaboration measurements, but in disagreement with the Mainz Collaboration extractions and the Particle Data Book (CODATA 2010–2014) results. For the neutron, we find $\langle r_n^2 \rangle = -0.089 \pm 0.002(\text{stat.}) \pm 0.002(\text{sys.}) \text{ fm}^2$, which is $\approx 23.6\%$ below the value obtained by the recent precise measurements of the neutron $G_E^n(Q^2)$ form factor at low- Q^2 utilizing the connection between the $N \rightarrow \Delta$ quadrupole transitions and $G_E^n(Q^2)$, and $\approx 29.4\%$ below the new adjusted $\langle r_n^2 \rangle$ world data value.

DOI: 10.1103/PhysRevC.109.065201

I. INTRODUCTION

The elastic nucleon (proton and neutron) electromagnetic form factors $G_{(E,M)}^{(p,n)}(Q^2)$ are key ingredients to characterize the internal structure of the nucleon, and extend our understanding of hadronic physics and quantum chromodynamics (QCD). They are also key inputs to many studies and analyses aimed at understanding composite particles and their nuclear structures [1–5]. However, despite decades of efforts spent in studying the nucleon internal structure, there are still a number of puzzles surrounding the nucleon such as its form factors and their ratios $R_{(p,n)} = \mu_{(p,n)} G_E^{(p,n)} / G_M^{(p,n)}$, nucleon spin, and its root-mean-square (RMS) charge radius. The recent proton $\langle r_p \rangle$ value as measured using the ultrahigh precise muonic hydrogen μH Lamb shift measurements of $\langle r_p \rangle = 0.84184(67) \text{ fm}$ [6] and $\langle r_p \rangle = 0.84087(39) \text{ fm}$ [7] are significantly smaller, with a discrepancy of $(5\text{--}7)\sigma$, than the recommended values established by the Particle Data Book (CODATA 2010–2014) of $\langle r_p \rangle = 0.8775(51) \text{ fm}$, which are compiled from ep scattering, and ordinary hydrogen spectroscopy measurements. For the proton, such a discrepancy suggests that the proton is 12% smaller in volume and denser than previously believed. That in turn led to a significant reassessment of the methods and analyses utilized in $\langle r_p \rangle$ extraction, as well as the consideration of possible physics beyond the standard model, such as possible undetected new

particles/forces and quantum gravity, as potential solutions to such a discrepancy. Among other possible resolutions of the “ $\langle r_p \rangle$ puzzle” are the prescriptions of the radiative corrections applied to the elastic ep scattering cross section $\sigma_R(\varepsilon, Q^2)$; missing higher-order radiative corrections to $\sigma_R(\varepsilon, Q^2)$, in particular missing two-photon exchange (TPE) effect; missing structures in the proton’s $G_{(E,M)}^p(Q^2)$ form factors and e^+e^- proton sea; inaccurate atomic physics calculations; experimental issues (either μH or ep measurements are wrong); experiments not measuring the same $\langle r_p \rangle$ quantity, or measuring it in different frames; underestimated uncertainties in ep extractions; and/or bad radius extractions, which also include the adopted functional forms fitted and the four-momentum transferred squared Q^2 range of data used in many several previous analyses and fitting procedures. See Refs. [8–26] and references therein for details.

In addition, the experimentally reported proton’s form factors ratio R_p as measured using the Rosenbluth separation method [27] and the high- Q^2 recoil polarization method [28–30], in the one-photon-exchange (OPE) or Born-approximation, differs almost by a factor of 3 at high Q^2 [31–33]. Such a discrepancy has also suggested a systematic difference between the two techniques, and was attributed to missing TPE corrections to σ_R , which were thoroughly studied theoretically [34–79], phenomenologically [80–107], and experimentally [108–112] in the last few years. See Refs. [113–115] for detailed reviews. However, many extractions of the proton charge and magnetic radius based on ep scattering measurements have relied on calculating the

*Corresponding author: issam.qattan@ku.ac.ae

radius based on the $G_{(E,M)}^p Q^2$ slope at $Q^2 = 0$, which requires the use of TPE corrected $G_{(E,M)}^p$ form factors, which many extractions did not incorporate [116–122]. Moreover, the data Q^2 range and choice of the adopted functional forms fitted used in $\langle r_p \rangle$ extractions, and the quantification of the statistical and systematic uncertainties, constitute big challenges, which in turn led to a significant reassessment and reevaluation of the methods and analyses utilized in $\langle r_p \rangle$ extraction.

Experimentally, different ep scattering experiments were carried out to precisely extract the charge radius of the proton. See Refs. [123,124] and references therein for details. Recently, Xiong *et al.* (PRad I Collaboration) [125] performed high-precision ep elastic scattering measurements to extract G_E^p in the range (2×10^{-4}) – 0.06 GeV², and then fitted G_E^p to a rational function of order (1,1) with two normalization parameters n_1 and n_2 , which correspond to the two separate beam energy values used: $G_E^p(Q^2) = n_1(1 + p_1 Q^2)/(1 + p_2 Q^2)$ and $n_2(1 + p_1 Q^2)/(1 + p_2 Q^2)$. They reported $\langle r_p \rangle = 0.831 \pm 0.007(\text{stat.}) \pm 0.012(\text{sys.})$ fm, which is consistent with the muonic Lamb shift results, but smaller than previous ep measurements. High-precision measurements of the recoil-polarization ratio $R_p = \mu_p G_E^p/G_M^p$ in the range of $0.30 < Q^2 < 0.7$ GeV² were performed by Zhan *et al.* [126]. They combined their extracted R_p and other few R_p world data to perform a new global fit of the proton's form factors in order to extract the charge radius. They obtained $\langle r_p \rangle = 0.875 \pm 0.010$ fm. Two Mainz experiments were performed to extract the proton's charge radius: Bernauer *et al.* (Mainz A1 2010 Collaboration) [122] carried out unpolarized ep measurements in the range $0.004 \leq Q^2 \leq 1.0$ GeV². The cross sections were fitted to several Padé and spline functional forms, and the $G_{(E,M)}^p$ form factors were extracted up to $Q^2 = 1.0$ GeV². They quoted $\langle r_p \rangle = 0.879(5)(\text{stat.})(4)(\text{sys.})(2)(\text{model})(4)(\text{group})$ fm. Mihovilovic *et al.* [127] performed a new Mainz experiment using the initial-state-radiation technique (Mainz ISR experiment) to measure ep elastic scattering cross sections in the range $0.001 \leq Q^2 \leq 0.004$ GeV². They reported $\langle r_p \rangle = 0.870 \pm 0.014(\text{stat.}) \pm 0.024(\text{sys.}) \pm 0.003(\text{model})$.

There are also many dedicated theoretical and phenomenological studies aimed at calculating and extracting the nucleon charge radius. Lorenz *et al.* [128] used a dispersive approach to reanalyze the Mainz 2010 data, where they included both the proton's and neutron's world data. They obtained $\langle r_p \rangle = 0.84 \pm 0.01$. In later analysis, Lorenz *et al.* [43] applied TPE correction and some physical constraints to the Mainz data, and used an improved dispersive approach with improved spectral functions and obtained $\langle r_p \rangle = 0.840(0.828\text{--}0.855)$ fm with 3σ uncertainties. Lee *et al.* [129] performed a new global analysis of ep elastic scattering world data including the Mainz 2010 data, where they applied model-independent constraints based on the form factors analyticity. They obtained $\langle r_p \rangle = 0.895(20)/0.916(24)$ fm with the inclusion/exclusion of the Mainz 2010 data. Hill *et al.* [130] performed model-independent conformal mapping in terms of $z(t, t_{\text{cut}}, t_0)$, where $t = Q^2$, $t_{\text{cut}} = 4m_p^2$ (m_p = pion physical mass). The G_E^p form factor was expanded as a

function of z , suppressing higher-order terms in z , and fitted to ep scattering datasets, yielding $\langle r_p \rangle = 0.870 \pm 0.023(\text{stat.}) \pm 0.012(\text{sys.})$. Lin *et al.* [131] used an improved dispersive approach with an improved two-pion continuum, Roy-Steiner analysis of pion-nucleon scattering, and obtained $\langle r_p \rangle = 0.838 \pm 0.005 \pm 0.004$ fm. Horbatsch and Hessels [132] reanalyzed the Mainz 2010 data using a dipole functional form and a linear fit to a conformal-mapping variable. They reported $\langle r_p \rangle$ values ranging 0.84–0.89 fm. Horbatsch *et al.* [133] included higher moments fixed to values obtained from chiral perturbation theory, and obtained $\langle r_p \rangle = 0.855(11)$ fm. Griffioen *et al.* [134] reanalyzed the Mainz 2010 data using a continued fractional function to map G_E^p with the assumption that G_E^p is monotonically falling and inflectionless function. They reported $\langle r_p \rangle = 0.840(16)$ fm. In a new analysis, Arrington and Sick [135] performed a new global analysis and obtained $\langle r_p \rangle = 0.879(11)$ fm. Sick [118] performed detailed analysis aimed at reducing the model dependence related to extrapolation and its impact on the slope $dG_E^p/dQ^2|_{Q^2 \rightarrow 0}$. Different form factors parametrizations for data obtained before 2010 were used, and a value of $\langle r_p \rangle = 0.887(12)$ fm was reported. Cui *et al.* [136] extracted $\langle r_p \rangle$ using the PRad I and the Mainz 2010 data. They used a statistical sampling approach based on the Schlessinger point method. They reported $\langle r_p \rangle = 0.838 \pm 0.005(\text{stat.}) (0.856 \pm 0.014(\text{stat.}))$ fm when using the PRad I (Mainz 2010) data, and including only data up to $Q^2 = 0.014$ GeV². Combining these two values, they reported $r_E = 0.847 \pm 0.008(\text{stat.})$ fm. Alarcon *et al.* [137] combined chiral effective field theory and a dispersion analysis approach, and reported $\langle r_p \rangle = 0.844(7)$ fm. In another analysis, Alarcon *et al.* [138] used the above mentioned analysis and the Mainz 2010 data, and reported $\langle r_p \rangle = 0.842 \pm 0.002(\text{fit}) \pm 0.010(\text{theory})$ and no change on the $\langle r_p \rangle$ value when the PRad I data were included. Kraus *et al.* [139] reported that using truncated polynomials to fit G_E^p would give too small values for $\langle r_p \rangle$. Atac *et al.* [140] performed global analysis of the Dirac $F_1^{(u,d)}$ form factors data to extract the proton $\langle r_p \rangle$ and neutron $\langle r_n \rangle$ charge radius. Assuming isospin symmetry, flavor separation of the Dirac $F_1^{(u,d)}$ form factors up to $Q^2 = 1.0$ GeV² was performed, and the 2D up- and down-quark RMS transverse radius was calculated based on fits to $F_1^{(u,d)}$ using $\langle b_{(u,d)}^2 \rangle = [-4/F_1^{(u,d)}(0)]dF_1^{(u,d)}(Q^2)/dQ^2|_{Q^2 \rightarrow 0}$. They reported $\langle r_p \rangle = 0.852 \pm 0.002(\text{stat.}) \pm 0.009(\text{sys.})$ fm, and neutron $\langle r_n \rangle = -0.122 \pm 0.004(\text{stat.}) \pm 0.010(\text{sys.})$ fm². However, when they exclude the the PRad I data, they still obtain a value of $\langle r_p \rangle = 0.857(13)$ fm. Shintani *et al.* [141] calculated the nucleon $G_{(E,M)}^{(p,n)}$ form factors without the disconnected diagram on a $(10.8 \text{ fm})^4$ lattice at the physical point in $2 + 1$ flavor QCD (LQCD), which were used to calculate the nucleon charge radius. For the proton, they obtained a value of $\langle r_p \rangle = 0.858(13)(35)$ fm, which is amid experimental values, but for the neutron they obtained $\langle r_n \rangle = -0.047(20)(18)$ fm², which is far from the experimental values as a result of not including the disconnected diagram. Vaziri and Shojaei [142] calculated the nucleon charge radius based on different modified generalized parton distributions (GPDs) functions of the extended Regge and modified Gaussian ansatz models. For the proton, they obtained $\langle r_p \rangle$ values ranging from 0.857 to

0.942 fm, and for the neutron their $\langle r_n^2 \rangle$ ranged from -0.1004 to -0.1559 fm^2 .

The neutron also suffers similar discrepancy. Unlike the proton, there is no atomic method possible to extract $\langle r_n^2 \rangle$, and therefore $\langle r_n^2 \rangle$ extraction is more difficult and challenging. In addition, the absence of a free neutron target severely limits the electron scattering method, and all $\langle r_n^2 \rangle$ extractions have been limited and based on neutron-electron scattering length measurements, where low-energy neutrons are scattered by electrons bound in diamagnetic atoms. The compiled measurements listed in the Particle Data Group (PDG) show discrepancies, with $\langle r_n^2 \rangle$ taking on values ranging from $\langle r_n^2 \rangle = -0.114 \pm 0.003 \text{ fm}^2$ to $\langle r_n^2 \rangle = -0.134 \pm 0.009 \text{ fm}^2$. There are many speculations on the possible sources of such a discrepancy, which is unsolved to date. They include the effect of electrical polarizability and resonance corrections. See Refs. [140,143] and references therein for details. In addition to the experimental issues discussed above, many phenomenological $\langle r_n^2 \rangle$ extractions were performed by calculating the slope of G_E^n at $Q^2 = 0$, or by constructing the up- and down-quark flavor-dependent Dirac and Pauli $F_{1,2}^{(u,d)}$ form factors [140], which requires reliable parametrizations of the nucleon $G_{(E,M)}^{(p,n)}$ and $F_1^{(u,d)}$ form factors.

II. EXTRACTION OF THE NUCLEON CHARGE RADIUS

Many of the phenomenological and theoretical nucleon charge radius extractions and calculations discussed above have relied on calculating the nucleon charge radius based on the slopes of $G_E^{(p,n)}$ at $Q^2 = 0$ assuming that the nucleons have three-dimensional (3D) charge distributions, which is problematic and not a well defined concept as the size of the nucleon is larger than its Compton wavelength, making it impossible to well localize the center-of-mass in three spatial dimensions [144–146]. In addition, many extractions and calculations have used either uncorrected TPE proton's form factors or incorporated TPE prescriptions that are driven mainly by the many assumptions and constraints applied, or used complex and empirical TPE functional forms. Relevant to radius extraction, TPE corrections have a significant impact even at low Q^2 and in particular at low ε , where the correction decreases with increasing Q^2 for $\varepsilon > 0.4$, and for $\varepsilon < 0.3$ the correction increases first and then decreases, reaching a fractional correction to the cross section of $\approx 2\%$, which will impact both form factors and radius extraction. See Refs. [129,147] and references therein for details. In addition, several studies have suggested that TPE corrections to the proton charge radius themselves have a correction due to the proton charge radius [8,49,121,148–150]. While these corrections are not large enough to explain the proton charge radius discrepancy, they are still important and too large to be neglected. Inclusion of these corrections reduces the proton charge radius measured by Mainz [122] by $\approx 0.8\%$ for the lowest beam energy of 180 MeV and taking the $Q^2 \rightarrow 0$ limit. At large Q^2 values, the reduced cross section σ_R is dominated by the magnetic form factor $G_M^p(Q^2)$, and the TPE corrections are most significant at small ε and can reach $\approx -6\%$ at $Q^2 = 6.0 \text{ GeV}^2$ [115]. However, as the charge radius is

extracted in the limit $Q^2 \rightarrow 0$, all previous extractions focused mainly on the low- Q^2 range, limiting the extraction up to $Q^2 = 1.0 \text{ GeV}^2$ as data taken at $Q^2 > 1.0 \text{ GeV}^2$ are rather insensitive to radius extraction. Therefore, it would be difficult at this point to quantify the impact of TPE corrections on the radius extraction when large- Q^2 data are included. Moreover, and relevant to this work, the recent nucleon charge radius extractions by Atac *et al.* [140] used $F_1^{(u,d)}$ data and a fitting range up to $Q^2 = 1.0 \text{ GeV}^2$. In their analysis, mixed low- Q^2 proton's G_E^p data from unpolarized elastic ep σ_R and polarized R_p measurements combined with R_n data from polarization measurements were used to construct the ratio $F_2^{(p,n)}/F_1^{(p,n)} = (1 - R_{(p,n)}/\mu_{(p,n)})/(\tau + R_{(p,n)}/\mu_{(p,n)})$, and then used it to extract the Dirac $F_1^{(u,d)}$ form factors using $F_1^u = 2F_1^p + F_1^n$ and $F_1^d = 2F_1^n + F_1^p$. For both the the proton and neutron, world data come from different measurements and do not match in Q^2 . Therefore, for each of the proton and neutron, world data are analyzed using a parametrization for its isospin partner counterpart. Different Sachs form factors parametrizations including those from Ref. [151] and updated parametrizations of the most recent Sachs form factors world data using the functional forms adapted in Ref. [116] were utilized in order to extract the flavor-dependent $F_1^{(u,d)}$ form factors at a common Q^2 value. However, it is not clear whether or not their updated parametrizations have used TPE corrected proton's form factors. For the neutron G_E^n form factor, two parametrizations were adapted: (1) the functional form of Galster [152] $G_E^n(Q^2) = (1 + Q^2/A)^{-2} B\tau/(1 + C\tau)$ with three free parameters A , B , and C , without constraining A to $\Lambda^2 = 0.71 \text{ GeV}^2$ as in Galster's case, and (2) the sum of two dipoles $G_E^n(Q^2) = [A(1 + Q^2/B)^{-2} - A(1 + Q^2/C)^{-2}]$ with three fitting parameters A , B , and C .

The extracted Dirac $F_1^{(u,d)}$ form factors were fitted globally up to $Q^2 = 1.0 \text{ GeV}^2$ to several different functional forms including rational, polynomials, polynomial \times dipole, and polynomial+dipole of different orders, and used to extract the 2D up- and down-quark RMS transverse radii $\langle b_{(u,d)}^2 \rangle$ needed for radius extractions. Unlike unpolarized ep σ_R measurements, polarized R_p data are insensitive to TPE corrections [108], and therefore using mixed proton's G_E^p data will impact both $F_1^{(u,d)}$ form factors [93,95,153] and consequently the nucleon charge radius value, as TPE corrections to σ_R at low- Q^2 values, although they are expected to be small, still need to be applied. In addition, the low- Q^2 G_E^p data from Mainz 2010 [122] and PRad I [125] used in the analysis were not corrected for TPE corrections, and suffer systematic differences due to normalizations uncertainties, yielding different G_E^p values in the overlapping region [122,125,154]. However, Coulomb corrections based on the prescription of Tsai [155] were only applied to the Mainz 2010 data.

Rational functions of Q^2 with different orders have been used widely [104,116,124,125,140,156], and shown to be effective in predicting the Q^2 dependence of the nucleon $G_{(E,M)}^{(p,n)}$ form factors over a wide range of Q^2 with a proper behavior for both $Q^2 \rightarrow 0$ and $Q^2 \rightarrow \infty$. At low- Q^2 a power series with even powers of Q is desirable, and at high- Q^2 dimensional scaling rules require that the degree of the denominator is

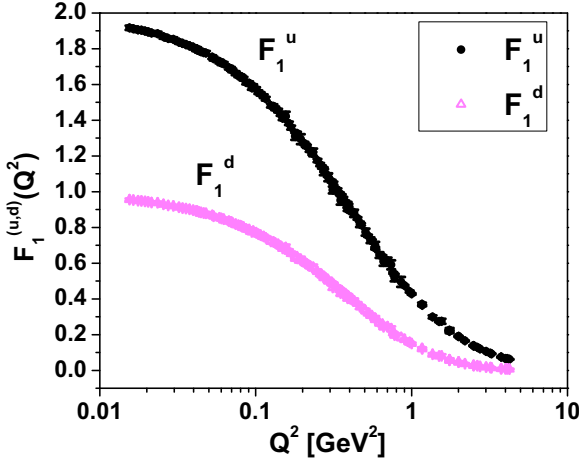


FIG. 1. The F_1^u (solid black circle) and F_1^d (open magenta triangle) Dirac form factors as extracted from Refs. [93,95]. See text for details.

larger than that of the numerator to ensure that $G_{E,M}^p \propto Q^{-4}$ for large Q^2 [116]. In the work of Atac *et al.* [140], rational functions of order $(n, m) = (1, 1), (2, 1), (4, 3), (5, 4)$, and $(6, 5)$ were used to fit $F_1^{(u,d)}(Q^2)$ up to $Q^2 = 1.0$ GeV², in addition to other functional forms as discussed before. However, the rational functional forms used suggest that $F_1^{(u,d)}(Q^2) \propto Q^2$ for the most part, with the power of the numerator is always higher than that of the denominator. While all the fitted functional forms used seem to fit the data in the low- Q^2 data range considered, most of these functional forms will not capture and predict the Q^2 dependence of the $F_1^{(u,d)}$ form factors over the entire Q^2 range of data.

Below we discuss the procedure used to extract the nucleon charge radius. Assuming isospin and charge symmetry and neglecting the strange quarks' contributions, we use the Dirac flavor-separated up- and down-quark $F_1^{(u,d)}(Q^2)$ form factors data as extracted in Refs. [93,95] covering the range of $0.0155 < Q^2 < 4.250$ GeV² and shown in Fig. 1. In our analysis, we only include the low- Q^2 data from Mainz 2010 [122] but not the PRad I [125] data to avoid dealing with any systematic differences due to normalizations uncertainties, which yield different G_E^p values in the overlapping Q^2 region. In the analysis of Refs. [93,95], world data on ep elastic scattering reduced cross sections σ_R covering the range of $0.0155 \leq Q^2 \leq 4.250$ GeV² were fitted to the TPE parametrization of Borisjuk and Kobushkin (BK) [86] in order to extract the proton's true $G_{(E,M)}^p(Q^2)$ form factors and the TPE parameter $a(Q^2)$. In the BK parametrization, σ_R is expressed as

$$\sigma_R = G_M^2 \left[1 + \frac{\varepsilon}{\tau} R^2 + 2a(Q^2)(1 - \varepsilon) \right], \quad (1)$$

where the TPE contribution to σ_R is defined as $F(\varepsilon, Q^2) = 2a(Q^2)G_M^2(1 - \varepsilon)$, and the TPE parameter $a(Q^2)$ is a function of Q^2 . The proton's form factors ratio $R = R_p/\mu_p = G_E^p/G_M^p$ was constrained to its value as given by a new and improved parametrization: $R_p(Q^2) = [1/1 + 0.1430Q^2 - 0.0086Q^4 + 0.0072Q^6]$, along with its associated uncertainty $\delta_{R_p}^2(Q^2) = \{(0.006)^2 + [0.015 \ln(1 + Q^2)]^2\}$, with Q^2

in GeV². At each Q^2 value, the proton's magnetic $G_M^p(Q^2)$ form factor and the TPE parameter $a(Q^2)$ were extracted as the parameters of the fit. The proton's G_E^p form factor was then determined using $G_E^p = RG_M^p$. For the neutron, an updated parametrization to $G_M^n(Q^2)$ world data, including the CLAS high- Q^2 data [157] up to $Q^2 = 8.0$ GeV², using the functional form as Kelly's [116], but with a modified parameters $a_1 = 5.857$, $b_1 = 18.74$, $b_2 = 54.07$, and $b_3 = 177.73$, was used. The uncertainty on G_M^n was taken to be the same as in the original Kelly fit, using the full error correlation matrix, with an error band fairly consistent with the experimental uncertainties with the CLAS [157] data included. For G_E^n extraction, the fit to $R_n = \mu_n G_E^n/G_M^n$ from Riordan *et al.* [158] and the new G_M^n parametrization were used. The uncertainties on G_E^n were determined using the full error correlation for R_n and G_M^n , which yielded uncertainties on G_E^n significantly smaller than the uncertainties on the individual measurements as a result of the simple functional form of the R_n parametrization. To account for this, the uncertainty on G_E^n was scaled up by a factor of 2 to provide more realistic uncertainties on the flavor-separated results. The Dirac nucleon $F_1^{(p,n)}(Q^2)$ form factors were first extracted using

$$F_1^{(p,n)} = \frac{G_E^{(p,n)} + \tau_{(p,n)} G_M^{(p,n)}}{1 + \tau_{(p,n)}}, \quad (2)$$

and then used to extract the Dirac flavor-separated $F_1^{(u,d)}(Q^2)$ form factors [159,160] using

$$F_1^u = (2F_1^p + F_1^n), \quad F_1^d = (F_1^p + 2F_1^n), \quad (3)$$

where $\tau_{(p,n)} = Q^2/4M_{(p,n)}^2$. In our analysis, the Dirac $F_1^{(u,d)}(Q^2)$ form factors were first fitted globally and then separately to rational functional forms of different orders (n, m) and fitting parameters using $F_1^{(u,d)}(Q^2) = [a_0^{(u,d)} + \sum_{i=1}^n a_i^{(u,d)} Q^{2i}] / [1 + \sum_{j=1}^m b_j^{(u,d)} Q^{2j}]$ covering the full range of $0.0155 \leq Q^2 \leq 4.250$ GeV². During the fitting process, we used the same functional form and order for $F_1^{(u,d)}(Q^2)$, and constrained $F_1^{(u,d)}(0) = a_0^{(u,d)}$ to 2.0 (1.0), respectively. For the global fitting, $F_1^{(u,d)}$ share the same fitting parameters, and the following rational functional forms were used: $(n = 1, m = 1)$, $(n = 1, m = 2)$, $(n = 1, m = 3)$, and $(n = 1, m = 4)$. These functions are labeled as R_2, R_3, R_4 , and R_5 , and correspond to two, three, four, and five fitting parameters, respectively. For the separate fittings, the same rational functional forms were used to fit $F_1^{(u,d)}$ separately. These functions are labeled as $(R_2 \times R_2), (R_3 \times R_3), (R_4 \times R_4)$, and $(R_5 \times R_5)$, and correspond to two, three, four, and five fitting parameters for each form factor. Again, $F_1^{(u,d)}(0)$ or $a_0^{(u,d)}$ were constrained to 2.0 (1.0) for F_1^u (F_1^d). As the charge radius is extracted in the limit $Q^2 \rightarrow 0$, where all previous extractions have focused mainly on low- Q^2 data range limiting the extraction up to $Q^2 = 1.0$ GeV², we will follow the same procedure outlined in Refs. [122,140] and perform the radius extraction within a finite and extended Q^2 range limiting the extraction up to $Q^2 = 1.0$ GeV² to avoid any sensitivity to all nucleon form factors as Q^2 increases. However, we still investigate any model dependence of the

fits that might be associated with the inclusion of high- Q^2 data points by extending the fitting range above $Q^2 = 1.0 \text{ GeV}^2$ up to $Q^2 = 4.25 \text{ GeV}^2$. Therefore, the extracted charge radius based on both the limited and extended Q^2 ranges will be shown for comparison. For each functional form, we repeated the fitting procedure by varying/reducing the upper-cutoff Q^2 value, $Q_i^2 = Q_{\text{cutoff}}^2$, of the fitting range A_i in a descending order as $A_i = [0.0155, Q_i^2] \text{ GeV}^2$ ($i = 1, \dots, 7$) and $Q_i^2 = 4.25, 2.50, 1.00, 0.75, 0.50, 0.25$, and 0.10 GeV^2 , respectively, in order to investigate the impact of inclusion of high- Q^2 data, fitting procedure, data fitting range, and convergence of the fitted functions on the stability and precision of the extracted charge radius. For example, $A_1 = [0.0155, 4.25] \text{ GeV}^2$, $A_2 = [0.0155, 2.50] \text{ GeV}^2$, \dots , $A_7 = [0.0155, 0.10] \text{ GeV}^2$. For each functional form and fitting range, the transverse mean-square radii of the two-dimensional (2D) transverse quark charge distributions $\langle b_{(u,d)}^2 \rangle$ were calculated based on the slopes of $F_1^{(u,d)}(Q^2)$ at $Q^2 = 0$ [123,144–146] using

$$\langle b_{(u,d)}^2 \rangle = \frac{-4}{F_1^{(u,d)}(0)} \left. \frac{dF^{(u,d)}(Q^2)}{dQ^2} \right|_{Q^2 \rightarrow 0}, \quad (4)$$

and then used to extract the charge radius through the model-independent relations defined for the proton as

$$\langle r_p^2 \rangle = 2\langle b_u^2 \rangle - \frac{1}{2}\langle b_d^2 \rangle + \frac{3\kappa_N}{2M_N^2}, \quad (5)$$

and for the neutron as

$$\langle r_n^2 \rangle = \langle b_d^2 \rangle - \langle b_u^2 \rangle + \frac{3\kappa_N}{2M_N^2}, \quad (6)$$

where κ_N and M_N are the anomalous magnetic moment and mass of the nucleon, respectively. In our analysis, we set κ_p (κ_n) and M_p (M_n) to 1.792847 (−1.913042) and 0.938272 (0.939565) GeV for the proton (neutron), respectively. For “each” rational fitted function, the charge radius values $\langle r_p \rangle$ and $\langle r_n^2 \rangle$ were extracted by combining the results of the seven or five different fitting ranges (A_1 – A_7) or (A_3 – A_7). We follow the same procedure of Refs. [122,140], where for “each” functional form fitted, the final $\langle r_p \rangle$ ($\langle r_n^2 \rangle$) value was taken as the weighted-average value, weighted by the statistical uncertainty σ_i (weight = $w_i = 1/\sigma_i^2$) on each $\langle r_p \rangle$ ($\langle r_n^2 \rangle$) value obtained for each of the seven or five different fitting ranges (A_1 – A_7) or (A_3 – A_7). The systematic uncertainty on the final $\langle r_p \rangle$ ($\langle r_n^2 \rangle$) value for “each” of the functional forms used was determined by calculating the weighted variance of the seven or five fitting ranges (A_1 – A_7) or (A_3 – A_7) results. The final combined $\langle r_p \rangle$ ($\langle r_n^2 \rangle$) value is taken as the weighted-average of all functional forms final results, weighted by the total uncertainty (statistical+systematic uncertainties added in quadrature), and with a systematic uncertainty as the weighted variance.

III. RESULTS AND DISCUSSION

In this section, we present the results obtained for the proton $\langle r_p \rangle$ and neutron $\langle r_n^2 \rangle$ charge radius based on both the global and separate fitting approaches using the four different

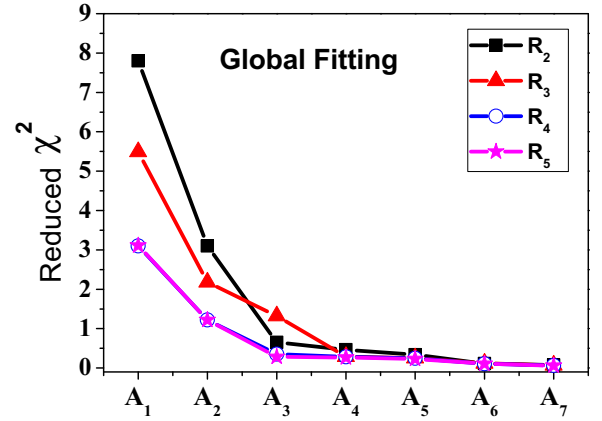


FIG. 2. The obtained reduced χ^2 (χ_v^2) value for the fitted functions (R_2 – R_5) over the fitting ranges (A_1 – A_7) based on the global fitting approach. The solid lines through the data points are guides to the eye.

rational functional forms discussed above over the (A_1 – A_7) and (A_3 – A_7) fitting ranges. In addition, we investigate any model dependence of the fits that might be associated with extending the data range above $Q^2 = 1.0 \text{ GeV}^2$ by truncating Q_{cutoff}^2 at 1.0 GeV^2 , and including only the results of the five (A_3 – A_7) fitting ranges to calculate the final and final combined $\langle r_p \rangle$ and $\langle r_n^2 \rangle$ values. Figure 2 shows the obtained reduced- χ^2 (χ_v^2) value of the fit for each function fitted over the fitting ranges (A_1 – A_7). The χ_v^2 value for each fitted function decreased with decreasing Q_{cutoff}^2 value, or fitting range, taking on values of $\chi_v^2 > 3.0$ for the A_1 fitting range and down to $\chi_v^2 = 0.1$ for the A_7 fitting range. The best fits are achieved when the fitting ranges are limited to (A_3 – A_7) with $0.1 \leq \chi_v^2 \leq 1.2$. Figure 3 shows the global fitting results for the different fitted functions used and for all (A_1 – A_7) fitting ranges. Both $\langle r_p \rangle$ and $\langle r_n^2 \rangle$ values obtained using all fitted functions over the A_1 and A_2 fitting ranges show a clear trend away from those obtained over the (A_3 – A_7) fitting ranges, where the charge radius values reach high stability. All fitted functions yield high statistical precision over the (A_1 – A_7) fitting ranges, where the statistical uncertainty tends to increase with decreasing Q_{cutoff}^2 value. For each function, the final $\langle r_p \rangle$ ($\langle r_n^2 \rangle$) value, taken as the weighted average of the (A_1 – A_7) and (A_3 – A_7) fitting ranges results, is also shown with the inner (outer) error bars indicating the statistical (total) uncertainty on the final charge radius. The higher $\langle r_p \rangle$ ($\langle r_n^2 \rangle$) value obtained over both the A_1 and A_2 fitting ranges seems to be highly correlated with the number of fitting parameters used in each fitting function, which in turn affects the χ_v^2 value obtained. Functions with fewer fitting parameters seem to yield larger $\langle r_p \rangle$ ($\langle r_n^2 \rangle$) and χ_v^2 values over the A_1 and A_2 fitting ranges, suggesting an underfitting of the data in these two fitting ranges. On the other hand, the small χ_v^2 values obtained for the low- Q^2 fitting ranges suggest that the fitted functions are possibly overfitting the data as rational functions and in particular those of higher order provide rather too much flexibility to adequately fit the data in the low- Q^2 range.

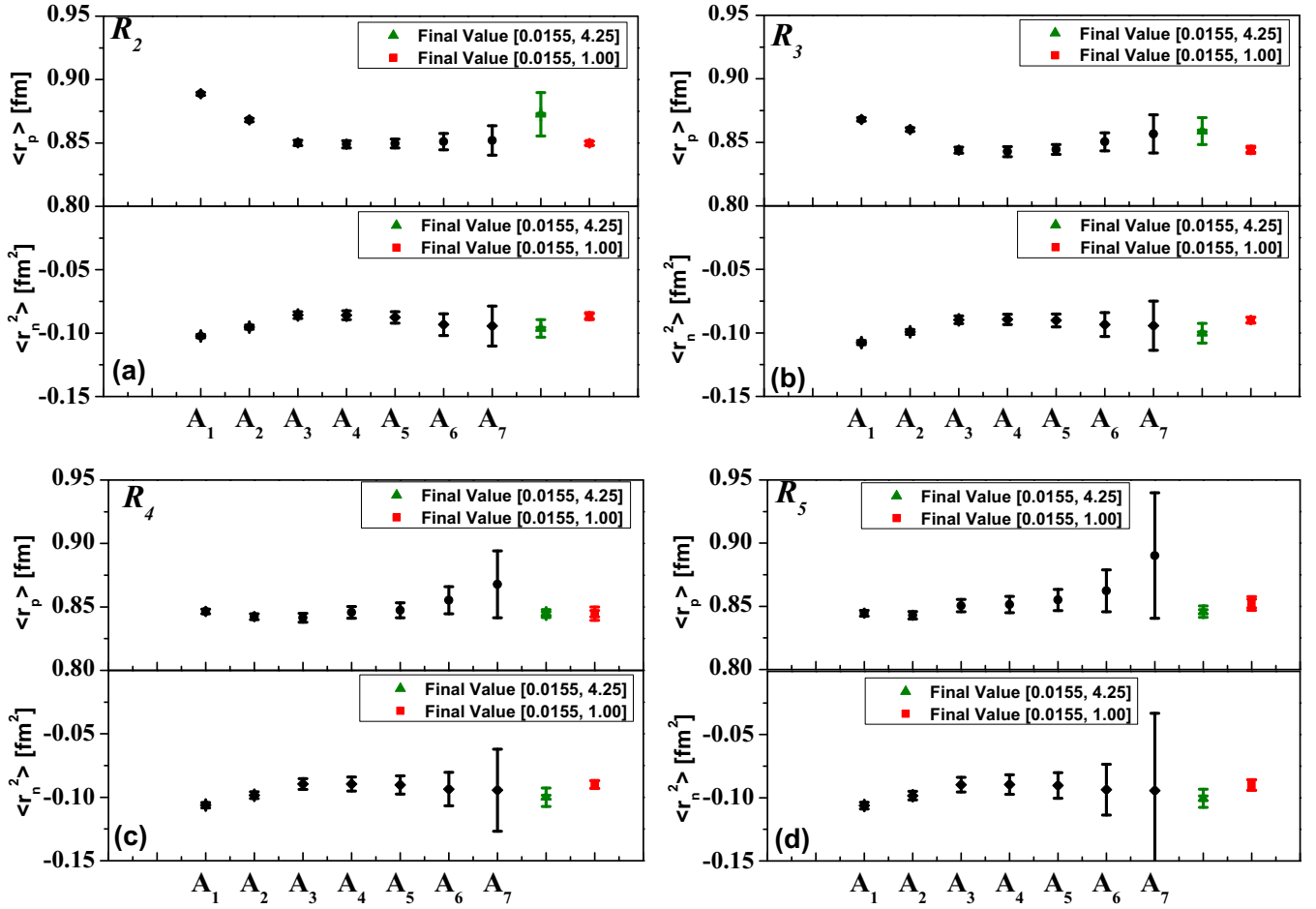


FIG. 3. The proton ($\langle r_p \rangle$) (top: solid black circle) and neutron ($\langle r_n^2 \rangle$) (bottom: solid black diamond) charge radius as extracted based on the global fitting approach utilizing the different fitted functions for the (A_1 – A_7) fitting range. For each fitted function, the final extracted nucleon charge radius for the (A_1 – A_7) (solid dark green diamond) and (A_3 – A_7) (solid red square) fitting ranges is also shown. The inner (outer) error bars indicate the statistical (total) uncertainty. See text for details.

Figure 4 shows the separate fitting results. Again, all fitted functions, with the exception of the $R_2 \times R_2$ fitted function, which yields lower $\langle r_n^2 \rangle$ values over the A_1 and A_2 fitting ranges, yield high stability in their results for both $\langle r_p \rangle$ and $\langle r_n^2 \rangle$ over the (A_1 – A_7) fitting ranges, but with relatively larger statistical uncertainties compared to those obtained using the global fitting approach. Note that the $R_5 \times R_5$ fitted function yields unphysical and large $\langle r_n^2 \rangle$ and statistical uncertainty over the A_1 fitting range, and so will not be shown in Fig. 4. However, we did not exclude this value when calculating the final and final combined $\langle r_n^2 \rangle$ values over the (A_1 – A_7) fitting range. A similar trend for χ^2_v was also observed when each of $F_1^{(u,d)}$ form factors was fitted separately, and the best fits were also achieved when the fitting ranges were limited to (A_3 – A_7). The final $\langle r_p \rangle$ ($\langle r_n^2 \rangle$) value is also shown for each fitted function. Figures 5 and 6 show the final and final combined proton and neutron charge radius values as extracted based on both fitting approaches utilizing the different fitted functions and for both the (A_1 – A_7) and (A_3 – A_7) fitting ranges. The final combined charge radius values are also listed in Table I. The global fitting approach clearly provides higher stability and precision for the final and final combined proton and neutron charge

radius values compared to those obtained using the separate fitting approach, and when the fitting ranges are limited to (A_3 – A_7). For the proton, inclusion of the A_1 and A_2 fitting ranges, based on the global (separate) fitting results, decreases the final combined charge radius by $\approx 0.24\%$ ($\approx 0.35\%$) but increases both the statistical and systematic uncertainties. On the other hand, this is not the case for the neutron, as the final combined charge radius is highly sensitive to both the fitting procedure and fitting range. Inclusion of the A_1 and A_2 fitting ranges increases the neutron final combined charge radius by $\approx 11.24\%$ ($\approx 9.68\%$) based on the global (separate) fitting results, and increases the statistical uncertainty in the case of the global fitting. In addition, changing the fitting procedure from global to separate but keeping the same fitting range decreases the proton final combined charge radius by $\approx 0.24\%$ and $\approx 0.12\%$ for the (A_1 – A_7) and (A_3 – A_7) fitting ranges, respectively. On the other hand, for the neutron, increases in the final combined charge radius by $\approx 3.00\%$ and $\approx 5.00\%$ are seen for the (A_1 – A_7) and (A_3 – A_7) fitting ranges, respectively. The reduction in $\langle r_n^2 \rangle$ value and based on both fitting procedures and for all fitted functions used is attributed to the fact that the difference ($\langle b_d^2 \rangle - \langle b_u^2 \rangle$) in Eq. (6) is always

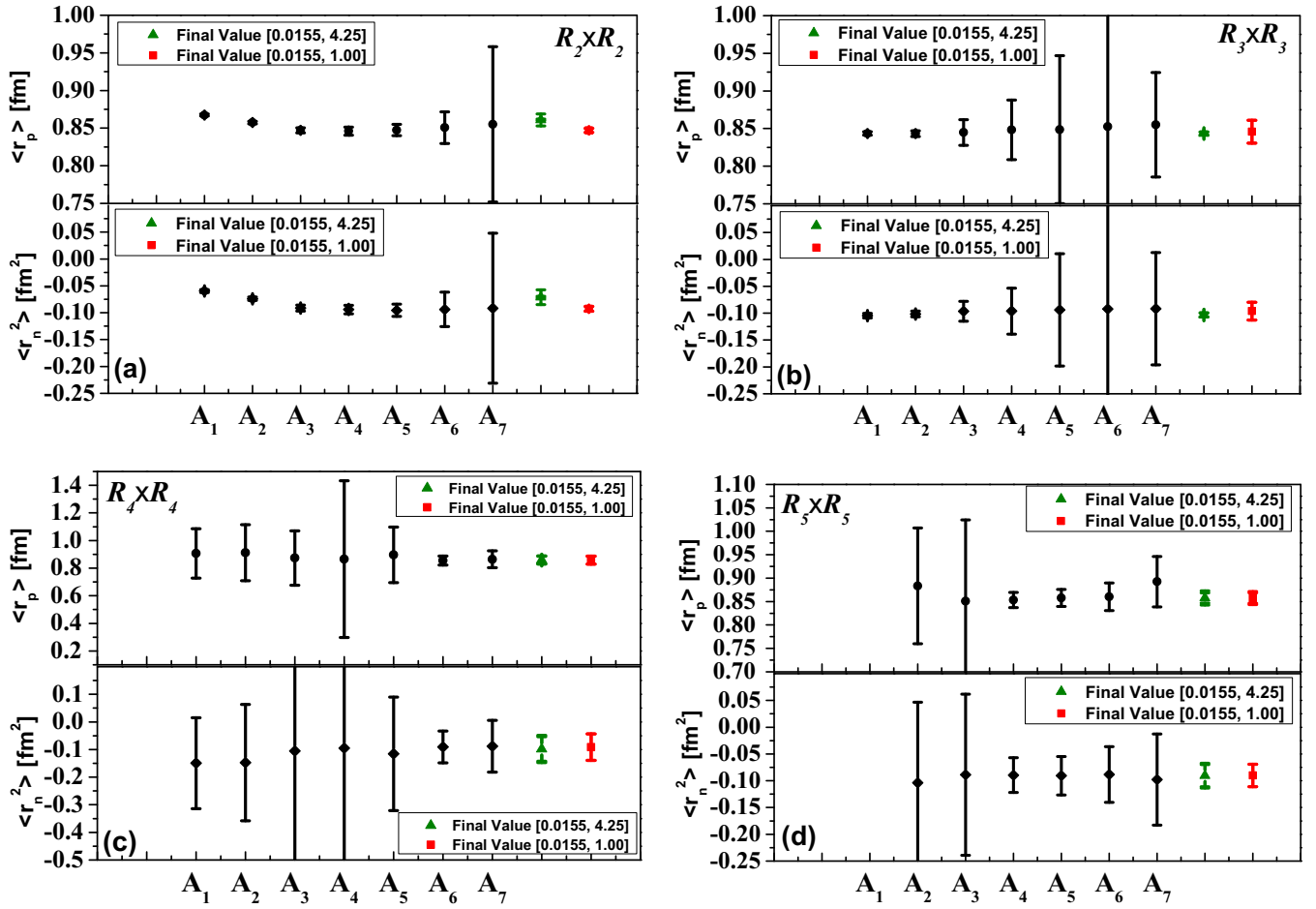


FIG. 4. The proton $\langle r_p \rangle$ (top: solid black circle) and neutron $\langle r_n^2 \rangle$ (bottom: solid black diamond) charge radius as extracted based on the separate fitting approach utilizing the different fitted functions for the (A_1 – A_7) fitting range. For each fitted function, the final extracted nucleon charge radius for the (A_1 – A_7) (solid dark green diamond) and (A_3 – A_7) (solid red square) fitting ranges are also shown. The inner (outer) error bars indicate the statistical (total) uncertainty. See text for details.

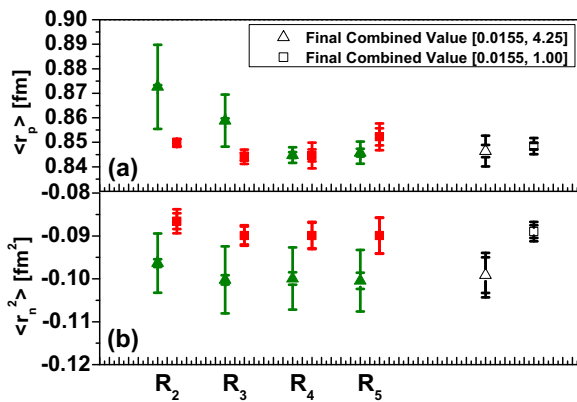


FIG. 5. The final proton $\langle r_p \rangle$ (top) and neutron $\langle r_n^2 \rangle$ (bottom) charge radius as extracted based on the global fitting approach utilizing the different fitted functions for the (A_1 – A_7) (solid dark green triangle) and (A_3 – A_7) (solid red square) fitting ranges. The final combined values are shown by open black diamonds and open black squares for the (A_1 – A_7) and (A_3 – A_7) fitting ranges, respectively. The inner (outer) error bars indicate the statistical (total) uncertainty. See text for details.

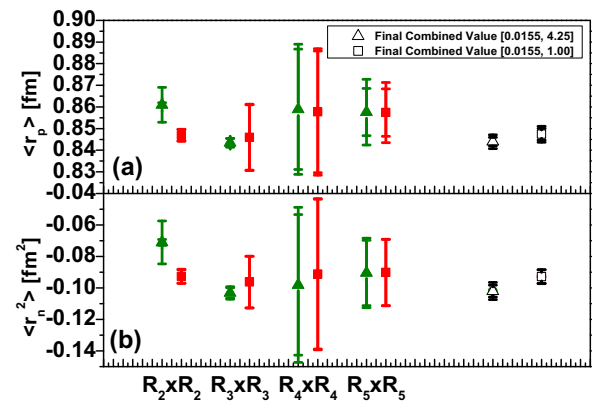


FIG. 6. The final proton $\langle r_p \rangle$ (top) and neutron $\langle r_n^2 \rangle$ (bottom) charge radius as extracted based on the separate fitting approach utilizing the different fitted functions for the (A_1 – A_7) (solid dark green triangle) and (A_3 – A_7) (solid red square) fitting ranges. The final combined values are shown by open black diamonds and open black squares for the (A_1 – A_7) and (A_3 – A_7) fitting ranges, respectively. The inner (outer) error bars indicate the statistical (total) uncertainty. See text for details.

TABLE I. The final combined proton $\langle r_p \rangle$ and neutron $\langle r_n^2 \rangle$ charge radii based on both the global and separate fits results.

Fit type	Fitting range	$\langle r_p \rangle$ fm	$\langle r_n^2 \rangle$ fm ²
Global fit	(A ₁ –A ₇)	$0.846 \pm 0.003(\text{stat.}) \pm 0.006(\text{sys.})$	$-0.099 \pm 0.004(\text{stat.}) \pm 0.002(\text{sys.})$
Global fit	(A ₃ –A ₇)	$0.848 \pm 0.002(\text{stat.}) \pm 0.003(\text{sys.})$	$-0.089 \pm 0.002(\text{stat.}) \pm 0.002(\text{sys.})$
Separate fit	(A ₁ –A ₇)	$0.844 \pm 0.002(\text{stat.}) \pm 0.003(\text{sys.})$	$-0.102 \pm 0.004(\text{stat.}) \pm 0.004(\text{sys.})$
Separate fit	(A ₃ –A ₇)	$0.847 \pm 0.003(\text{stat.}) \pm 0.003(\text{sys.})$	$-0.093 \pm 0.004(\text{stat.}) \pm 0.002(\text{sys.})$

positive and increases with decreasing Q^2 . Therefore, considering the impact of inclusion of high- Q^2 data, fitting procedure and fitting range, convergence of the fitted functions and χ^2_ν values obtained, and stability and precision of the final and final combined extracted charge radius values, we take the final combined $\langle r_p \rangle$ and $\langle r_n^2 \rangle$ values obtained based on the global fitting approach over the (A₃–A₇) fitting ranges as our final values for the nucleon charge radius.

Recently, Zhou *et al.* [154] carried out a complete reanalysis of the Mainz 2010 34 data sets of ep elastic scattering cross sections data with their 31 unconstrained normalization parameters up to $Q^2 = 0.50$ GeV² in order to understand the discrepancy on the G_E^p data extracted by the Mainz 2010 and PRad I Collaborations, as both experiments have an overlapping Q^2 range above $Q^2 = 0.0038$ GeV². They have concluded that the choice of their fitting function, rational (1,1), can shift the floating normalization factor, and significantly shift the extracted form factors, bringing the Mainz 2010 G_E^p form factor into agreement with the PRad I G_E^p data within uncertainties. Atac *et al.* [140] extracted $\langle r_p \rangle$ first by including the PRad I and Mainz 2010 G_E^p data, and obtained $\langle r_p \rangle = 0.852 \pm 0.002(\text{stat.}) \pm 0.009(\text{sys.})$ fm, and then by excluding the PRad I data but keeping the Mainz 2010 data, yielding $\langle r_p \rangle = 0.857(13)$ fm, which still smaller than the value obtained by the Mainz 2010 Collaboration [122]. They concluded that the radius extraction method followed by the Mainz 2010 Collaboration has, most likely, underestimated the underlying uncertainties, or failed to avoid any form of bias during the fitting process. The $F_1^{(u,d)}$ form factors data used in this work have included the low- Q^2 Mainz 2010 data, down to $Q^2 = 0.0155$ GeV², but not the PRad I data, and so the results we have obtained on $\langle r_p \rangle$ following the two fitting approaches are consistent with the results obtained by Refs. [140,154], and in agreement with the ultrahigh precise muonic hydrogen μH Lamb shift [6,7] and PRad I measurements [125], but in disagreement with the Mainz 2010 [122] and the CODATA values.

Recently, Atac *et al.* [143] experimentally extracted $\langle r_n^2 \rangle$ relying on extraction of G_E^n at low Q^2 utilizing the connection between the $N \rightarrow \Delta$ quadrupole transitions and G_E^n , and obtained $\langle r_n^2 \rangle = -0.110 \pm 0.008$ fm². As the PDG exhibited discrepancy on $\langle r_n^2 \rangle$ with values ranging from $\langle r_n^2 \rangle = -0.114 \pm 0.003$ fm² to $\langle r_n^2 \rangle = -0.134 \pm 0.009$ fm², they have provided a new weighted average value of the world data after including their new measurement and excluding the value provided in Ref. [161], adjusting the current particle data book value to $\langle r_n^2 \rangle = -0.1152 \pm 0.0017$ fm², and improving its uncertainty by $\approx 23.0\%$. Their result is also in agreement with $\langle r_n^2 \rangle$ based on the determination of the

deuteron structure radius based on chiral effective field theory [162], which utilizes atomic data for the difference between the deuteron and proton charge radius. Note, however, that their $\langle r_n^2 \rangle$ value based on their flavor-dependent Dirac form factors extractions [140] is $\approx 11.0\%$ higher than their new measured value. In comparison, our $\langle r_n^2 \rangle$ value is below the previous extractions based on the flavor-dependent of the Dirac $F_1^{(u,d)}$ form factors [140] by $\approx 37\%$, the new precise measurement of Ref. [143] by $\approx 23.6\%$, and the new adjusted $\langle r_n^2 \rangle$ world data by 29.4%.

IV. CONCLUSIONS

In conclusion, we have performed new extraction of the proton $\langle r_p \rangle$ and neutron $\langle r_n^2 \rangle$ charge radius utilizing the Dirac flavor-separated up- and down-quark $F_1^{(u,d)}(Q^2)$ form factors data from Refs. [93,95] covering the range $0.0155 < Q^2 < 4.250$ GeV². The Dirac $F_1^{(u,d)}(Q^2)$ from factors are first fitted globally and then separately to different rational functional forms of different orders (n, m). For each fitted functional form, the fitting procedure is repeated by varying the upper-cutoff Q^2 value in a descending order in order to investigate the impact of inclusion of high- Q^2 data, fitting procedure, data fitting range, and convergence of the fitted functions used on the stability and precision of the extracted charge radius. The nucleon charge radius are calculated using the two-dimensional (2D) transverse quark charge distributions based on the slopes of $F_1^{(u,d)}(Q^2)$ at $Q^2 = 0$ through the model-independent relations [144–146]. For the proton, our results suggest that inclusion of high- Q^2 data, the A₁ and A₂ fitting ranges, decreases the final combined charge radius by $\approx 0.24\%$ ($\approx 0.35\%$) but increases both the statistical and systematic uncertainties based on the global (separate) fitting results. On the other hand, for the neutron, the final combined charge radius is highly sensitive to both the fitting range and fitting procedure, where inclusion of the A₁ and A₂ fitting ranges increases the charge radius by $\approx 11.24\%$ ($\approx 9.68\%$) based on the global (separate) fitting results, but increases only the statistical uncertainty in the case of the global fitting. We have also investigated the impact of changing the fitting procedure from global to separate but keeping the same fitting range, and for the proton the final combined charge radius decreases by $\approx 0.24\%$ and $\approx 0.12\%$ for the (A₁–A₇) and (A₃–A₇) fitting ranges, respectively. For the neutron, the impact is larger, and the final combined charge radius increases by $\approx 3.00\%$ and $\approx 5.00\%$ for the (A₁–A₇) and (A₃–A₇) fitting ranges, respectively. We find that the global fitting approach over the fitting range (A₃–A₇) yields

the best charge radius with values of $\langle r_p \rangle = 0.848 \pm 0.002$ (stat.) ± 0.003 (sys.) and $\langle r_n^2 \rangle = -0.089 \pm 0.002$ (stat.) ± 0.002 (sys.). Our extracted $\langle r_p \rangle$ value is consistent with the results obtained by Refs. [140,154], and in excellent agreement with ultrahigh precise muonic hydrogen μH Lamb shift [6,7] and PRad I measurements [125], but in disagreement with the Mainz [122] and the CODATA results. On the other hand, our extracted $\langle r_n^2 \rangle$ is below the value obtained by the previous extractions based on the

flavor-dependent Dirac form factors [140], the new precise measurement of Ref. [143], and the new adjusted $\langle r_n^2 \rangle$ world data value.

ACKNOWLEDGMENT

The authors acknowledge the support provided by Khalifa University of Science and Technology.

-
- [1] W. U. Boeglin *et al.*, *Phys. Rev. Lett.* **107**, 262501 (2011).
 - [2] J. Arrington, N. Fomin, and A. Schmidt, *Annu. Rev. Nucl. Part. Sci.* **72**, 307 (2022).
 - [3] J. Arrington *et al.*, *Prog. Part. Nucl. Phys.* **127**, 103985 (2022).
 - [4] X. Jiang *et al.*, *Phys. Rev. Lett.* **98**, 182302 (2007).
 - [5] D. K. Hasell, R. G. Milner, R. P. Redwine, R. Alarcon, and H. Gao, *Annu. Rev. Nucl. Part. Sci.* **61**, 409 (2011).
 - [6] R. Pohl *et al.*, *Nature (London)* **466**, 213-116 (2010).
 - [7] A. Antognini *et al.*, *Science* **339**, 417 (2013).
 - [8] C. E. Carlson, *Prog. Part. Nucl. Phys.* **82**, 59 (2015).
 - [9] G. A. Miller, A. W. Thomas, J. D. Carroll, and J. Rafelski, *Phys. Rev. A* **84**, 020101(R) (2011).
 - [10] J.-P. Karr and L. Hilico, *Phys. Rev. Lett.* **109**, 103401 (2012).
 - [11] G. A. Miller, *Phys. Lett. B* **718**, 1078 (2013).
 - [12] C. E. Carlson and B. C. Rislow, *Phys. Rev. D* **86**, 035013 (2012).
 - [13] V. Barger, C.-W. Chiang, W.-Y. Keung, and D. Marfatia, *Phys. Rev. Lett.* **106**, 153001 (2011).
 - [14] V. Barger, C.-W. Chiang, W.-Y. Keung, and D. Marfatia, *Phys. Rev. Lett.* **108**, 081802 (2012).
 - [15] P. Brax and C. Burrage, *Phys. Rev. D* **83**, 035020 (2011).
 - [16] U. D. Jentschura, *Ann. Phys. (NY)* **326**, 516 (2011).
 - [17] B. Batell, D. McKeen, and M. Pospelov, *Phys. Rev. Lett.* **107**, 011803 (2011).
 - [18] D. Tucker-Smith and I. Yavin, *Phys. Rev. D* **83**, 101702(R) (2011).
 - [19] T. Mart and A. Sulaksono, *Phys. Rev. C* **87**, 025807 (2013).
 - [20] T. Friedmann, *Eur. Phys. J. C* **73**, 2299 (2013).
 - [21] L.-B. Wang and W.-T. Ni, *Mod. Phys. Lett. A* **28**, 1350094 (2013).
 - [22] R. Pohl, R. Gilman, G. A. Miller, and K. Pachucki, *Annu. Rev. Nucl. Part. Sci.* **63**, 175 (2013).
 - [23] E. Borie, *Ann. Phys. (NY)* **327**, 733 (2012).
 - [24] U. Jentschura and B. Wundt, *Eur. Phys. J. D* **65**, 357 (2011).
 - [25] R. Onofrio, *Europhys. Lett.* **104**, 20002 (2013).
 - [26] S. G. Karshenboim, D. McKeen, and M. Pospelov, *Phys. Rev. D* **90**, 073004 (2014).
 - [27] M. N. Rosenbluth, *Phys. Rev.* **79**, 615 (1950).
 - [28] N. Dombey, *Rev. Mod. Phys.* **41**, 236 (1969).
 - [29] A. I. Akhiezer and M. P. Rekalo, *Fiz. Elem. Chast. Atom. Yadra* **4**, 662 (1973) [*Sov. J. Part. Nucl.* **4**, 277 (1974)].
 - [30] R. G. Arnold, C. E. Carlson, and F. Gross, *Phys. Rev. C* **23**, 363 (1981).
 - [31] I. A. Qattan *et al.*, *Phys. Rev. Lett.* **94**, 142301 (2005).
 - [32] J. Arrington, C. Roberts, and J. Zanotti, *J. Phys. G* **34**, S23 (2007).
 - [33] C. Perdrisat, V. Punjabi, and M. Vanderhaeghen, *Prog. Part. Nucl. Phys.* **59**, 694 (2007).
 - [34] P. G. Blunden, W. Melnitchouk, and J. A. Tjon, *Phys. Rev. Lett.* **91**, 142304 (2003).
 - [35] P. G. Blunden, W. Melnitchouk, and J. A. Tjon, *Phys. Rev. C* **72**, 034612 (2005).
 - [36] S. Kondratyuk, P. G. Blunden, W. Melnitchouk, and J. A. Tjon, *Phys. Rev. Lett.* **95**, 172503 (2005).
 - [37] S. Kondratyuk and P. G. Blunden, *Phys. Rev. C* **75**, 038201 (2007).
 - [38] N. Kivel and M. Vanderhaeghen, *Phys. Rev. Lett.* **103**, 092004 (2009).
 - [39] N. Kivel and M. Vanderhaeghen, *Phys. Rev. D* **83**, 093005 (2011).
 - [40] N. Kivel and M. Vanderhaeghen, *J. High Energ. Phys.* **04** (2013) 029.
 - [41] O. Tomalak and M. Vanderhaeghen, *Eur. Phys. J. A* **51**, 24 (2015).
 - [42] O. Tomalak, *Eur. Phys. J. A* **55**, 64 (2019).
 - [43] I. T. Lorenz, Ulf-G. Meißner, H.-W. Hammer, and Y.-B. Dong, *Phys. Rev. D* **91**, 014023 (2015).
 - [44] Y. C. Chen, A. Afanasev, S. J. Brodsky, C. E. Carlson, and M. Vanderhaeghen, *Phys. Rev. Lett.* **93**, 122301 (2004).
 - [45] A. V. Afanasev, S. J. Brodsky, C. E. Carlson, Y. C. Chen, and M. Vanderhaeghen, *Phys. Rev. D* **72**, 013008 (2005).
 - [46] Y. M. Bystritskiy, E. A. Kuraev, and E. Tomasi-Gustafsson, *Phys. Rev. C* **75**, 015207 (2007).
 - [47] E. Tomasi-Gustafsson and G. I. Gakh, *Phys. Rev. C* **72**, 015209 (2005).
 - [48] D. Borisyuk and A. Kobushkin, *Phys. Rev. C* **74**, 065203 (2006).
 - [49] D. Borisyuk and A. Kobushkin, *Phys. Rev. C* **75**, 038202 (2007).
 - [50] D. Borisyuk and A. Kobushkin, *Phys. Rev. C* **78**, 025208 (2008).
 - [51] D. Borisyuk and A. Kobushkin, *Phys. Rev. D* **79**, 034001 (2009).
 - [52] D. Borisyuk and A. Kobushkin, *Phys. Rev. C* **86**, 055204 (2012).
 - [53] D. Borisyuk and A. Kobushkin, *Phys. Rev. C* **89**, 025204 (2014).
 - [54] D. Borisyuk and A. Kobushkin, *Phys. Rev. C* **92**, 035204 (2015).
 - [55] H. Q. Zhou, C. W. Kao, and S. N. Yang, *Phys. Rev. Lett.* **99**, 262001 (2007); **100**, 059903(E) (2008).
 - [56] H.-Q. Zhou, *Chin. Phys. Lett.* **26**, 061201 (2009).
 - [57] Hai-Qing Zhou and S. N. Yang, *Eur. Phys. J. A* **51**, 105 (2015).
 - [58] K. M. Graczyk and C. Juszczak, *J. Phys. G* **42**, 034019 (2015).
 - [59] K. M. Graczyk, *Phys. Rev. C* **88**, 065205 (2013).
 - [60] K. M. Graczyk, *Phys. Rev. C* **84**, 034314 (2011).

- [61] V. M. Braun, A. Lenz, and M. Wittmann, *Phys. Rev. D* **73**, 094019 (2006).
- [62] P. G. Blunden and W. Melnitchouk, *Phys. Rev. C* **95**, 065209 (2017).
- [63] O. Tomalak and M. Vanderhaeghen, *Eur. Phys. J. C* **78**, 514 (2018).
- [64] O. Tomalak, B. Pasquini, and M. Vanderhaeghen, *Phys. Rev. D* **96**, 096001 (2017).
- [65] O. Tomalak, *Eur. Phys. J. C* **77**, 517 (2017).
- [66] C. E. Carlson, M. Gorchtein, and M. Vanderhaeghen, *Phys. Rev. A* **95**, 012506 (2017).
- [67] O. Tomalak, and M. Vanderhaeghen, *Phys. Rev. D* **93**, 013023 (2016).
- [68] H.-Q. Zhou and S. N. Yang, *Phys. Rev. C* **96**, 055210 (2017).
- [69] H.-Q. Zhou and S. N. Yang, *JPS Conf. Proc.* **13**, 020040 (2017).
- [70] O. Koshchii and A. Afanasev, *Phys. Rev. D* **96**, 016005 (2017).
- [71] O. Koshchii and A. Afanasev, *Phys. Rev. D* **98**, 056007 (2018).
- [72] J. Ahmed, P. G. Blunden, and W. Melnitchouk, *Phys. Rev. C* **102**, 045205 (2020).
- [73] A. V. Gramolin and D. M. Nikolenko, *Phys. Rev. C* **93**, 055201 (2016).
- [74] R. J. Hill, *Phys. Rev. D* **95**, 013001 (2017).
- [75] R. E. Gerasimov and V. S. Fadin, *J. Phys. G* **43**, 125003 (2016).
- [76] C. E. Carlson, B. Pasquini, V. Pauk, and M. Vanderhaeghen, *Phys. Rev. D* **96**, 113010 (2017).
- [77] O. Tomalak, *Eur. Phys. J. C* **77**, 858 (2017).
- [78] V. L. Chernyak, A. A. Ogloblin, and I. Zhitnitsky, *Z. Phys. C* **42**, 569 (1989).
- [79] J. Ahmad, P. G. Blunden, and W. Melnitchouk, *Phys. Rev. C* **108**, 055202 (2023).
- [80] P. A. M. Guichon and M. Vanderhaeghen, *Phys. Rev. Lett.* **91**, 142303 (2003).
- [81] J. C. Bernauer *et al.* (A1 Collaboration), *Phys. Rev. C* **90**, 015206 (2014).
- [82] J. Arrington, *Phys. Rev. C* **69**, 032201(R) (2004).
- [83] I. A. Qattan, Ph.D. thesis, Northwestern University, 2005.
- [84] V. Tvaskis, J. Arrington, M. E. Christy, R. Ent, C. E. Keppel, Y. Liang, and G. Vittorini, *Phys. Rev. C* **73**, 025206 (2006).
- [85] D. Borisyuk and A. Kobushkin, *Phys. Rev. C* **76**, 022201(R) (2007).
- [86] D. Borisyuk and A. Kobushkin, *Phys. Rev. D* **83**, 057501 (2011).
- [87] J. Arrington, *Phys. Rev. C* **71**, 015202 (2005).
- [88] Y.-C. Chen, C.-W. Kao, and S.-N. Yang, *Phys. Lett. B* **652**, 269 (2007).
- [89] J. Guttman, N. Kivel, M. Meiziane, and M. Vanderhaeghen, *Eur. Phys. J. A* **47**, 77 (2011).
- [90] M. P. Rekalo and E. Tomasi-Gustafsson, *Eur. Phys. J. A* **22**, 331 (2004).
- [91] I. A. Qattan and A. Alsaad, *Phys. Rev. C* **83**, 054307 (2011); **84**, 029905(E) (2011).
- [92] I. A. Qattan, A. Alsaad, and J. Arrington, *Phys. Rev. C* **84**, 054317 (2011).
- [93] I. A. Qattan and J. Arrington, *Phys. Rev. C* **86**, 065210 (2012).
- [94] I. A. Qattan and J. Arrington, *Eur. Phys. J. WOC* **66**, 06020 (2014).
- [95] I. A. Qattan, J. Arrington, and A. Alsaad, *Phys. Rev. C* **91**, 065203 (2015).
- [96] I. A. Qattan, *Phys. Rev. C* **95**, 055205 (2017).
- [97] I. A. Qattan and J. Arrington, *J. Phys.: Conf. Ser.* **869**, 012053 (2017).
- [98] I. A. Qattan, *Phys. Rev. C* **95**, 065208 (2017).
- [99] I. A. Qattan, D. Homouz, and M. K. Riahi, *Phys. Rev. C* **97**, 045201 (2018).
- [100] I. A. Qattan and J. Arrington, *J. Phys.: Conf. Ser.* **1258**, 012007 (2019).
- [101] I. A. Qattan, S. P. Patole, and A. Alsaad, *Phys. Rev. C* **101**, 055202 (2020).
- [102] I. A. Qattan, *J. Phys.: Conf. Ser.* **1643**, 012192 (2020).
- [103] A. Schmidt, *J. Phys. G* **47**, 055109 (2020).
- [104] I. A. Qattan, A. Alsaad, and A. A. Ahmad, *Phys. Rev. C* **103**, 055202 (2021).
- [105] I. A. Qattan, A. Alsaad, and A. A. Ahmad, *Phys. Rev. C* **103**, 045202 (2021).
- [106] I. A. Qattan, *AIP Conf. Proc.* **2319**, 080007 (2021).
- [107] I. A. Qattan, *Phys. Rev. C* **107**, 045202 (2023).
- [108] M. Meiziane *et al.*, *Phys. Rev. Lett.* **106**, 132501 (2011).
- [109] D. Adikaram *et al.* (CLAS Collaboration), *Phys. Rev. Lett.* **114**, 062003 (2015).
- [110] D. Rimal *et al.* (CLAS Collaboration), *Phys. Rev. C* **95**, 065201 (2017).
- [111] I. A. Racheek *et al.* (VEPP-3 Collaboration), *Phys. Rev. Lett.* **114**, 062005 (2015).
- [112] B. S. Henderson *et al.* (OLYMPUS Collaboration), *Phys. Rev. Lett.* **118**, 092501 (2017).
- [113] J. Arrington, P. Blunden, and W. Melnitchouk, *Prog. Part. Nucl. Phys.* **66**, 782 (2011).
- [114] C. E. Carlson and M. Vanderhaeghen, *Annu. Rev. Nucl. Part. Sci.* **57**, 171 (2007).
- [115] A. Afanasev, P. G. Blunden, D. Hasell, and B. A. Raue, *Prog. Part. Nucl. Phys.* **95**, 245 (2017).
- [116] J. J. Kelly, *Phys. Rev. C* **70**, 068202 (2004).
- [117] J. J. Kelly, *Phys. Rev. C* **66**, 065203 (2002).
- [118] I. Sick, *Atoms* **6**, 2 (2018).
- [119] J. R. Arrington, *J. Phys. Chem. Ref. Data* **44**, 031203 (2015).
- [120] I. Sick, *Phys. Lett. B* **576**, 62 (2003).
- [121] P. G. Blunden and I. Sick, *Phys. Rev. C* **72**, 057601 (2005).
- [122] J. C. Bernauer *et al.* (A1 Collaboration), *Phys. Rev. Lett.* **105**, 242001 (2010).
- [123] H. Gao and M. Vanderhaeghen, *Rev. Mod. Phys.* **94**, 015002 (2022).
- [124] W. Xiong and C. Peng, *Universe* **9**, 182 (2023).
- [125] W. Xiong *et al.* (PRad I Collaboration), *Nature (London)* **575**, 147-150 (2019).
- [126] X. Zhan *et al.*, *Phys. Lett. B* **705**, 59-64 (2011).
- [127] M. Mihovilovic *et al.*, *Phys. Lett. B* **771**, 194-198 (2017).
- [128] I. T. Lorenz, H.-W. Hammer, and Ulf-G. Meissner, *Eur. Phys. J. A* **48**, 151-156 (2012).
- [129] G. Lee, J. R. Arrington, and R. J. Hill, *Phys. Rev. D* **92**, 013013 (2015).
- [130] R. J. Hill, G. Lee, P. Gil, and M. P. Solon, *Phys. Rev. D* **87**, 053017 (2013).
- [131] Y.-H. Lin, H.-W. Hammer, and Ulf-G. Meissner, *Phys. Lett. B* **816**, 136254 (2021).
- [132] M. Horbatsch and E. A. Hessels, *Phys. Rev. C* **93**, 015204 (2016).
- [133] M. Horbatsch, E. A. Hessels, and A. Pineda, *Phys. Rev. C* **95**, 035203 (2017).
- [134] K. Griffioen, C. Carlson, and S. Maddox, *Phys. Rev. C* **93**, 065207 (2016).

- [135] J. R. Arrington and I. Sick, *J. Phys. Chem. Ref. Data* **44**, 031204 (2015).
- [136] Z.-F. Cui, D. Binosi, C. D. Roberts, and S. M. Schmidt, *Phys. Rev. Lett.* **127**, 092001 (2021).
- [137] J. M. Alarcon, D. W. Higinbotham, C. Weiss, and Z. Ye, *Phys. Rev. C* **99**, 044303 (2019).
- [138] J. M. Alarcon, D. W. Higinbotham, and C. Weiss, *Phys. Rev. C* **102**, 035203 (2020).
- [139] E. Kraus, K. E. Mesick, A. White, R. Gilman, and S. Strauch, *Phys. Rev. C* **90**, 045206 (2014).
- [140] H. Atac, M. Constantinou, Z.-E. Meziani, M. Paolone, and N. Sparveris, *Eur. Phys. J. A* **57**, 65 (2021).
- [141] E. Shintani, Ken-Ichi Ishikawa, Y. Kuramashi, S. Sasaki, and T. Yamazaki, *Phys. Rev. D* **99**, 014510 (2019); **102**, 019902(E) (2020).
- [142] H. Vaziri and M. R. Shojaei, *Phys. Rev. C* **107**, 055204 (2023).
- [143] H. Atac, M. Constantinou, Z.-E. Meziani, M. Paolone, and N. Sparveris, *Nat. Commun.* **12**, 1759 (2021).
- [144] G. A. Miller, *Phys. Rev. Lett.* **99**, 112001 (2007).
- [145] G. A. Miller, *Phys. Rev. C* **99**, 035202 (2019).
- [146] R. Dupre, M. Guidal, S. Niccolai, and M. Vanderhaeghen, *Eur. Phys. J. A* **53**, 171 (2017).
- [147] J. Arrington, *J. Phys. G* **40**, 115003 (2013).
- [148] R. Lee and A. Milstein, [arXiv:1402.3054](https://arxiv.org/abs/1402.3054).
- [149] R. Rosenfelder, *Phys. Lett. B* **479**, 381 (2000).
- [150] M. Gorchtein, [arXiv:1406.1612](https://arxiv.org/abs/1406.1612).
- [151] Z. Ye *et al.*, *Phys. Lett. B* **777**, 8 (2018).
- [152] S. Galster *et al.*, *Nucl. Phys. B* **32**, 221 (1971).
- [153] G. D. Cates, C. W. de Jager, S. Riordan, and B. Wojtsekhowski, *Phys. Rev. Lett.* **106**, 252003 (2011).
- [154] J. Zhou, V. Khachatryan, H. Gao, S. Gorbaty, and D. W. Higinbotham, *Phys. Rev. C* **106**, 065505 (2022).
- [155] Y.-S. Tsai, *Phys. Rev.* **122**, 1898 (1961).
- [156] M. E. Christy *et al.* (GMp12 Collaboration), *Phys. Rev. Lett.* **128**, 102002 (2022).
- [157] J. Lachniet *et al.* (CLAS Collaboration), *Phys. Rev. Lett.* **102**, 192001 (2009).
- [158] S. Riordan *et al.*, *Phys. Rev. Lett.* **105**, 262302 (2010).
- [159] G. A. Miller, B. M. K. Nefkens, and I. Slaus, *Phys. Rep.* **194**, 1 (1990).
- [160] D. H. Beck and R. D. McKeown, *Annu. Rev. Nucl. Part. Sci.* **51**, 189 (2001).
- [161] Y. A. Aleksandrov, M. Vrana, G. J. Manrique, T. A. Machekchina, and L. N. Sedlakova, *Sov. J. Nucl. Phys.* **44**, 900 (1986); *Yad. Fiz.* **44**, 1384 (1986).
- [162] A. A. Filin, V. Baru, E. Epelbaum, H. Krebs, D. Moller, P. Reinert, *Phys. Rev. Lett.* **124**, 082501 (2020).